Supporting Information for

Living Plant-Assisted Recycling of Nano Gold into Murray Porous Carbon Electrode Materials

Jinling Li, Qianghong Wu, Huanzhong Zeng, Rong Zou, Jianzhou Niu, Junlong Chen, Hongjun Liu, Fen Ran*

State Key Laboratory of Advanced Processing and Recycling of Non-ferrous Metals, Department of Polymeric Materials Engineering, School of Material Science and Engineering, Lanzhou University of Technology, Lanzhou 730050, Gansu, China

**Corresponding Author: Dr. Prof. Fen Ran (ranfen@lut.edu.cn, or ranfen@163.com)*

Materials and Methods

Materials

Gold chloride tri-hydrate ($HAuCl_4 \cdot 3H_2O$) and silver nitrate ($AgNO_3$) were subscribed from *Aladdin Chemistry Co., Ltd. (Shanghai, China)*. Sodium citrate dihydrate ($Na_3C_6H_5O_7 \cdot 2H_2O$) was supplied by the *Tianjin Kaixin Chemical Reagent Company*. Sodium borohydride ($NaBH_4$) and ascorbic acid (AA) were purchased from *Shanghai Zhongqin Chemical Reagent Co., Ltd.* CetyltrimethylAmmoniumBromide (CTAB) and HEPES (pH=7.4) were ordered from *Shanghai Macklin Biochemical Co., Ltd.* Tomato plants were purchased from *Weifang (Shandong, China)*. All used chemicals were of analytical grade and without further decontamination. Twice-distilled water was used throughout the work.

Synthesis and Preparation

*Preparation of Different Shapes Au Nanoparticl*es

Synthesis of Au NPs: Add 508 μL of $HAuCl_4 \cdot 3H_2O$ (10 mM) solution into 35 mL H_2O, stir well, and when the temperature of the oil bath rises to 100 °C, quickly add 200 μL of 0.1 M sodium citrate, and continue to react for 30 min. After the reactant was cooled to room temperature, the Au NPs can be obtained by centrifuge washing with water and ethanol for 3 times at a rotational speed of 12, 000 r/min.[1]

Synthesis of Au Nanorods (Au NRs): Au NRs were synthesized using the silver ion-assisted seed-mediated method, as described previously.[2] Briefly, to first prepared a solution of spherical Au nanoparticle seeds, 250 μL of an aqueous 0.01 M solution of $HAuCl_4 \cdot 3H_2O$ was added into 7.5 mL of an aqueous 0.1 M CTAB solution in a test tube. The solution was gently mixed by inversion. Then, 0.6 mL of an aqueous 0.01 M ice-cold $NaBH_4$ solution was added all at once, followed by rapid inversion mixing for 2 min. The seed solution was kept in a water bath at 25 °C and was used at least 2 h after its preparation. To grow Au NRs, 600 μL of 0.01 M $HAuCl_4 \cdot 3H_2O$ and 90 μL of 0.01 M $AgNO_3$ were added into 14.25 mL of 0.1 M CTAB in a test tube, followed by gentle inversion mixing. 96 μL of 0.1 M ascorbic acid solution was then added and the resulting solution was mixed. Finally, 63 μL of the seed solution was added, the reaction mixture was gently mixed for 10 s, and then left undisturbed for at least 3 h.

Au Nanobipyramid (Au NBPs) Growth: The Au NBPs samples were prepared using the seed-mediated growth method, as described in the previous works.[3] Specifically, the citrate-stabilized seed solution was made by adding freshly prepared, ice-cold $NaBH_4$ solution (0.01 M, 0.15 mL) into an aqueous solution composed of

$HAuCl_4 \cdot 3H_2O$ (0.01 M, 0.125 mL), trisodium citrate (0.01 M, 0.25 mL), and water (9.625 mL) under vigorous stirring. The resultant seed solution was kept at room temperature for 2 h before use. The CTAB growth solution was prepared by sequential addition of $HAuCl_4 \cdot 3H_2O$ (0.01 M, 2 mL), $AgNO_3$ (0.01 M, 0.4 mL), HCl (1 M, 0.8 mL), and ascorbic acid (0.1 M, 0.32 mL) into a CTAB solution (0.1 M, 40 mL). The seed solution of 1 mL was then added to the growth solution, followed by gentle inversion mixing for 10 s. The reaction solution was left undisturbed overnight at room temperature.

Au Nanostars (Au NSs) Synthesis: Aqueous stock solution of HEPES (pH=7.4) with a concentration of 100 mM was prepared with ultrapure water. In a typical experiment, 100 mL of 100 mM HEPES was mixed with 150 mL of deionized water, followed by the addition of 5 mL of 10 mM $HAuCl_4 \cdot 3H_2O$ solution. Without shaking, the color of the solution changed from light yellow to slightly purple and finally to greenish blue within 30 min.[4]

To further simulate plant contamination experiments, the prepared nanoparticles were diluted into a colloidal solution of 100 $mg \cdot L^{-1}$. A control treatment containing no Au NPs was included.

Tomato Exposure Experience

The enriched plant for the test was tomato seedlings, and the variety was Century Chun Da Fen, which was purchased from Weifang, Shandong Province, and cultured for 50 days in advance. Seedlings of uniform size were selected and cleaned, and three seedlings were placed in each beaker. Each group was replicated twice. All seedlings were cultivated in the contaminated solution (100 $mg \cdot L^{-1}$ different shapes of Au colloidal solution) for 40 h.

Preparation of Murray Porous Carbon

After being cultivated in the contaminated solution for 40 h, the plants were harvested, and the roots and leaves of the plants were washed with deionized water. Part of the plants were frozen with liquid nitrogen and transferred to the refrigerator for storage to be tested. The other part was frozen in the refrigerator and dried in a freeze-dryer for 3 d, and then sealed in a ziplock bag after grinding for alternative use. To enhance the preservation of the Murray pore structure in plants, the dry biomass underwent pre-oxidation at 300 °C for 2 h in a Muffle furnace (air atmosphere) before carbonization.[5,6] The pre-oxidized samples were moved to the tube furnace, the secondary carbonization at 800 °C for 3 h under Ar_2 atm., and the oxidized samples were washed in distilled

water, and dried in the oven at 60 °C for 48 h. These Murray porous carbon composites were labeled as control, 3DC-Au NPs, 3DC-Au NRs, 3DC-Au NBPs, and 3DC-Au NSs groups, respectively.

Characterization

The content of gold was measured by an inductively coupled plasma optical emission spectrometer (ICP-OES, Leeman Prodigy 7) and ultraviolet-visible spectrophotometer (UV-Vis, 7230 G). Morphology and size of Au NPs with different shapes were observed by transmission electron microscopy (TEM). The surface morphology of the porous carbon was observed by scanning electron microscope (SEM), and the element distribution of the composites was characterized by transmission electron microscope mapping, and the scanning voltage was 5 kV. X-ray diffraction (XRD, Rigaku D/MAX 2400 diffractometer, Japan) with Cu *Kα* radiation (l¼ 1.5418Å) was used for the analysis of phase constitution. The molecular structure of the final composite carbon materials was characterized using a Fourier Transform Infrared Spectrometer (FTIR). The chemical composition and molecular structure of the substances were identified and analyzed using Raman spectroscopy, with a focus on the changes in the G band and D band of graphene. The variety and content of elements in the materials were analyzed by X-ray Photoelectron Spectroscopy (XPS). The specific surface area and pore size distribution of the samples were determined using Brunauer-Emmett-Teller (BET) multi-molecular adsorption theory and the Barrett-Joyner-Halenda (BJH) equation.

Electrochemical Measurements

All electrochemical studies, including cyclic voltammetry (CV), galvanostatic charging/discharging (GCD), and electrochemical impedance spectroscopy (EIS), were conducted using an electrochemical workstation (CHI660E, Shanghai, China) in a 6 M KOH aqueous electrolyte. A conventional three-electrode system was utilized to assess electrochemical performance, comprising the produced active material as the working electrode, a platinum foil as the counter electrode, and a mercuric oxide electrode as the reference electrode. The working electrode was created by combining the active material, conducting graphite, acetylene black, and poly(tetrafluoroethylene) emulsion in a weight ratio of 80:7.5:7.5:5 to create a uniform black paste. The resultant slurry was applied to a 1 cm^2 nickel foam current collector. After being dried in an oven at 60 °C for 12 hours, the nickel foam coated with active materials was subjected to a pressure of 10 MPa using a tablet press for 5 seconds to improve the adhesion between the active materials and the current collector. The mass loading of active material was 4 $mg \cdot cm^{-2}$.

The specific mass capacitance of an electrode, determined using the galvanostatic cycle test, was computed using the following equation:

$$C = (I \times \Delta t)/(m \times \Delta V) \quad (1)$$

Where *C (*$F \cdot g^{-1}$*), I (A), Δt (s), m (mg),* and *ΔV (V)* were the specific capacity, discharging current, discharging time, the mass of active material, and the potential drop during discharging process, respectively.

The energy and power density of the device were determined from the discharge curves at various current densities in accordance with equations (2) and (3):

$$E = C \times V^2/(2 \times 3.6)V^2 \quad (2)$$

$$P = E \times 3600/\Delta t \quad (3)$$

where *E (Wh·kg*$^{-1}$*), C (F·g*$^{-1}$*), V (V), P (W·kg*$^{-1}$*),* and *Δt (s)* were the energy density, specific capacitance, potential drop during discharging process, power density, and discharging time, respectively.

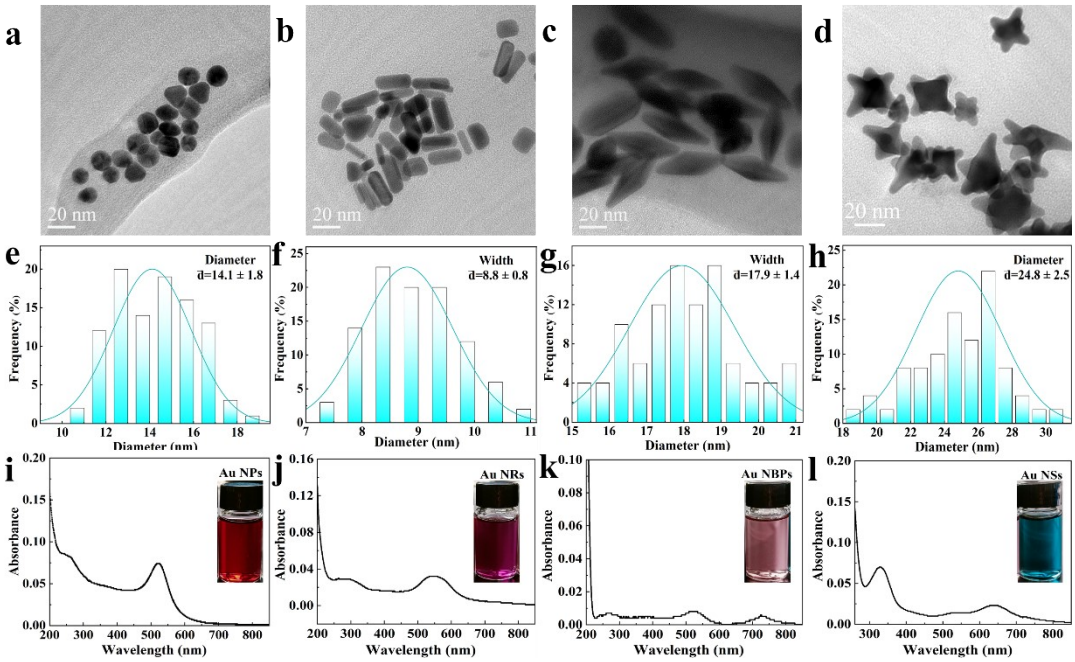

Figure S1 *Characterization of different shape Au NPs. a-d) TEM images of Au NPs, Au NRs, Au NBPs, and Au NSs, respectively. e-h) Au NPs, Au NRs, Au NBPs, and Au NSs particle size distribution, respectively. i-l) The UV-vis spectrometry of Au NPs, Au NRs, Au NBPs, and Au NSs, respectively. The inner illustrations are corresponding optical photos.*

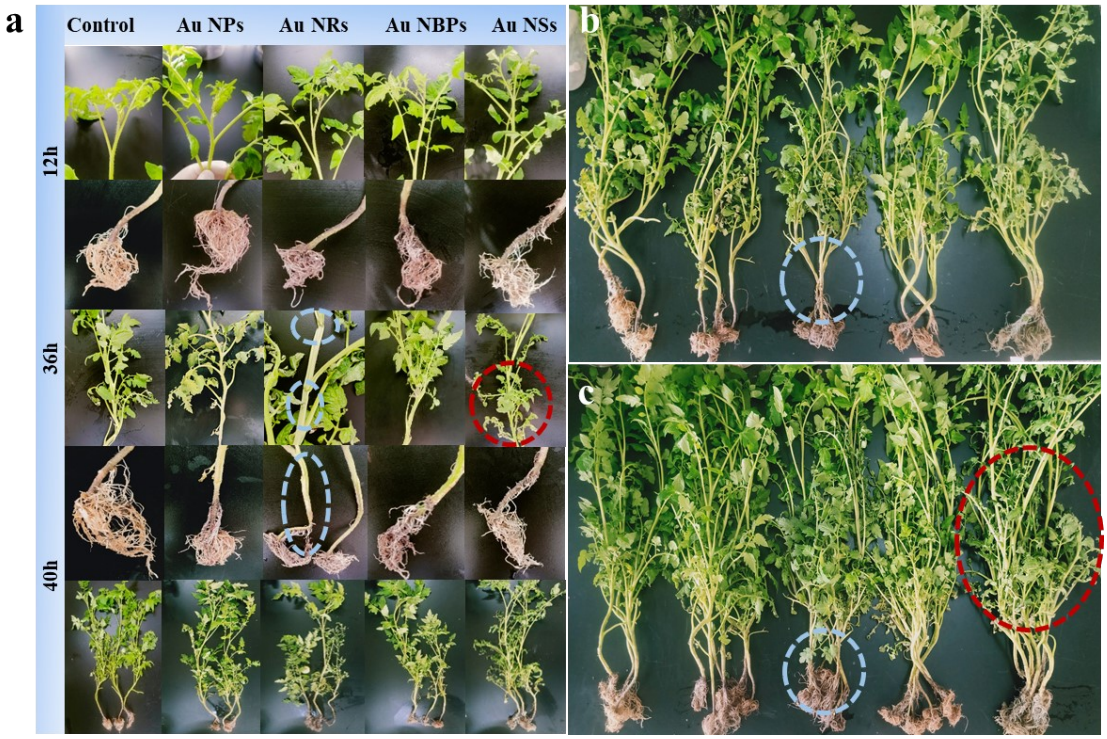

Figure S2 *Enrichment of Au NPs with different shapes in tomato and corresponding influence. a) Growth of Tomato contamination with different shapes of Au NPs in different periods. b) The overall growth status of one group of seedlings after 40 hours of pollution. c) Overall growth status of two groups of seedlings after 40 hours of pollution. The order from left to right in b) and b) diagrams is as follows: control, Au NPs, Au NRs, Au NBPs, and Au NSs. The blue dotted circle indicates the obvious wilting of tomato stems and the red dotted circles indicate the obvious dryness of tomato leaves.*

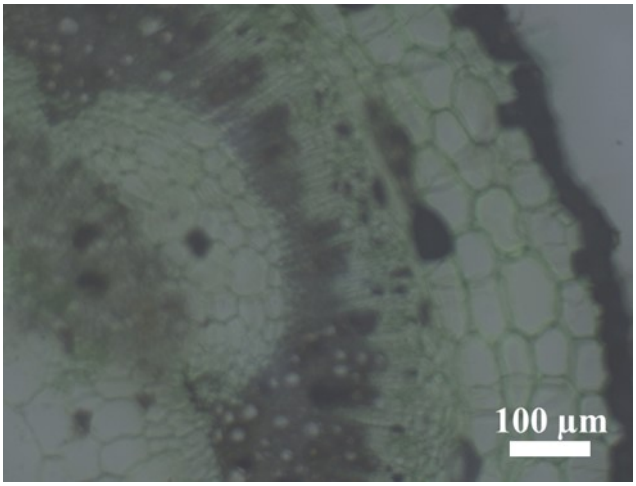

Figure S3 *The laser confocal microscopy picture of tomato stem (Au NRs).*

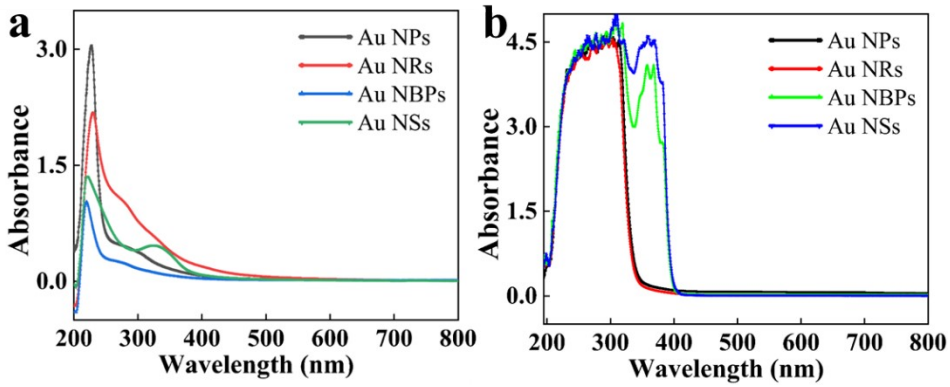

Figure S4 *a) Uv-vis absorption spectrum of residual solution. b) Absorption spectra of plants digestion after harvest.*

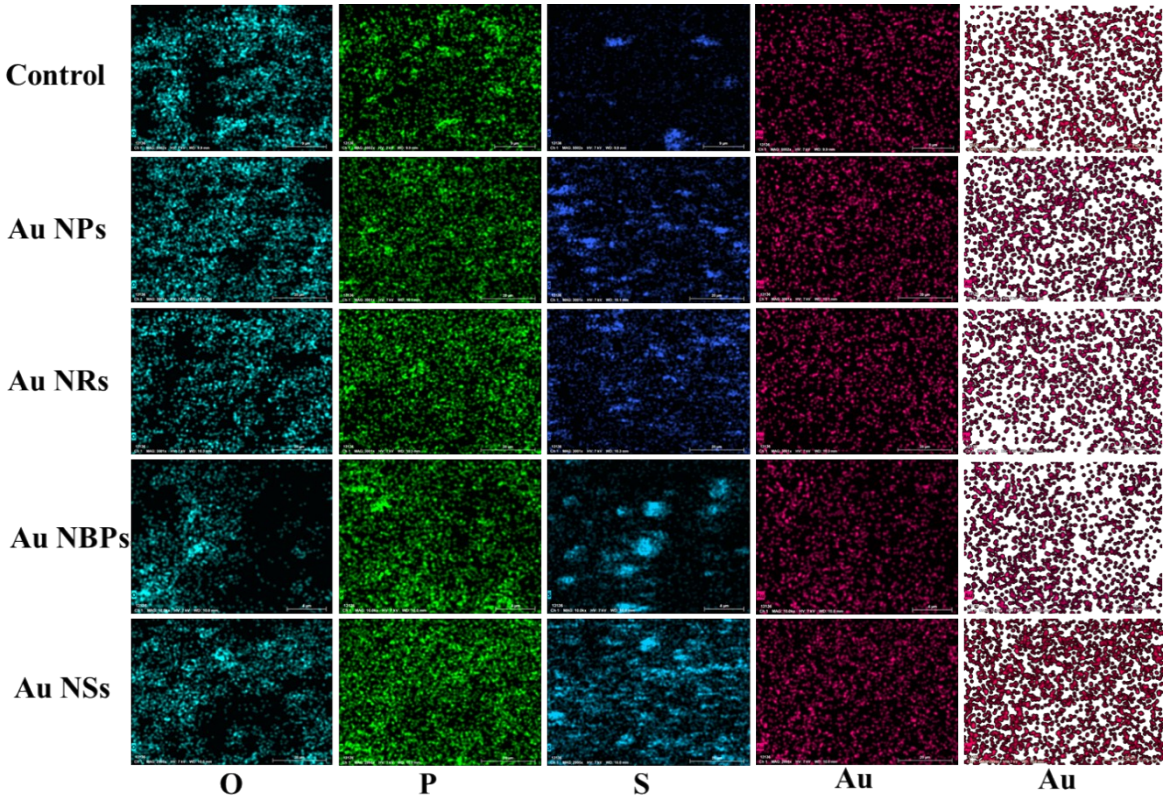

Figure S5. *SEM-EDS elemental mapping images of O, P, S, and Au for control, 3DC-Au NPs, 3DC-Au NRs, 3DC-Au NBPs, and 3DC-Au NSs, respectively.*

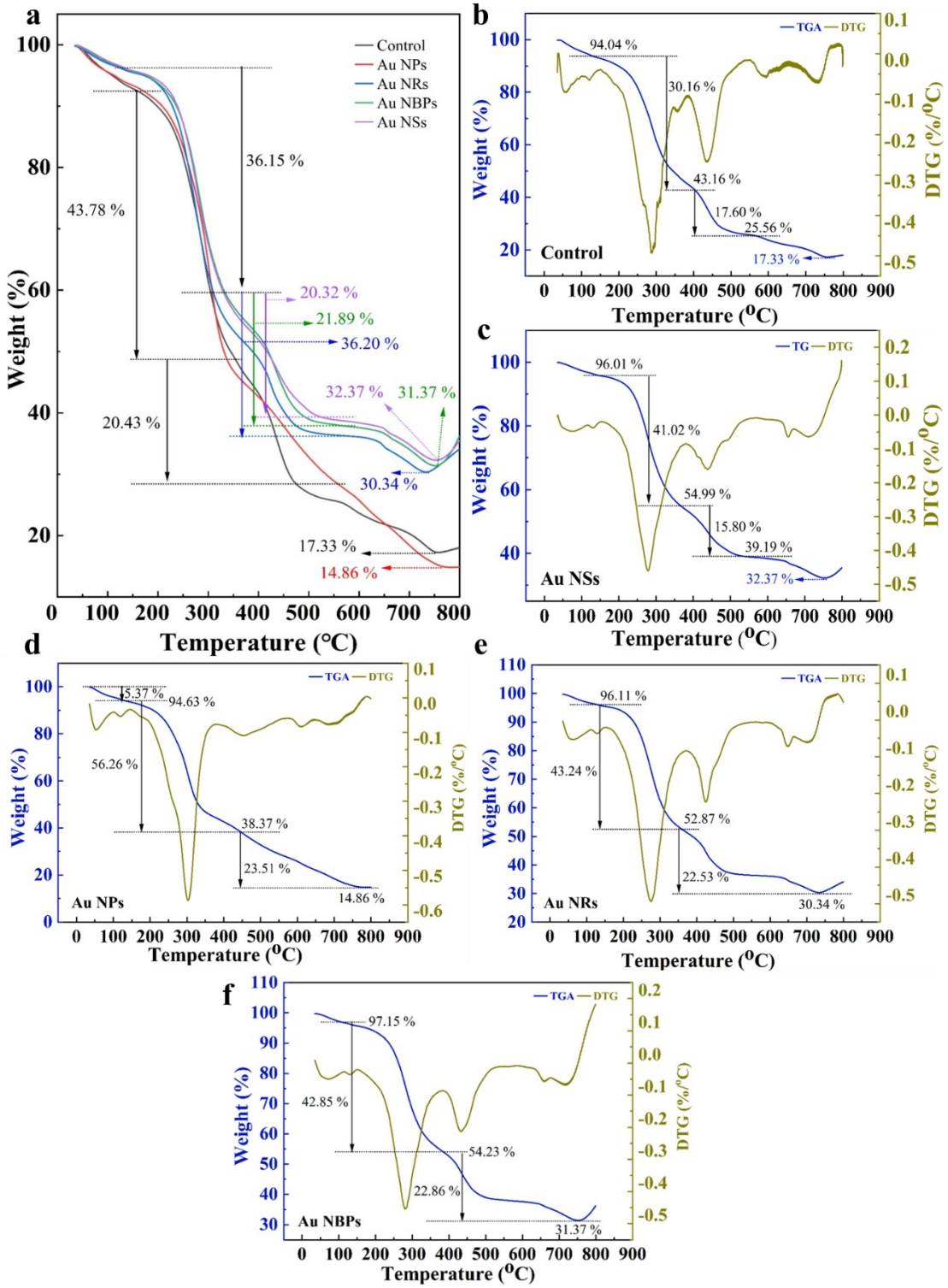

Figure S6 *TG/DTG curve of plants contaminate by control, Au NSs, Au NPs, Au NRs, and Au-NBPs, respectively.*

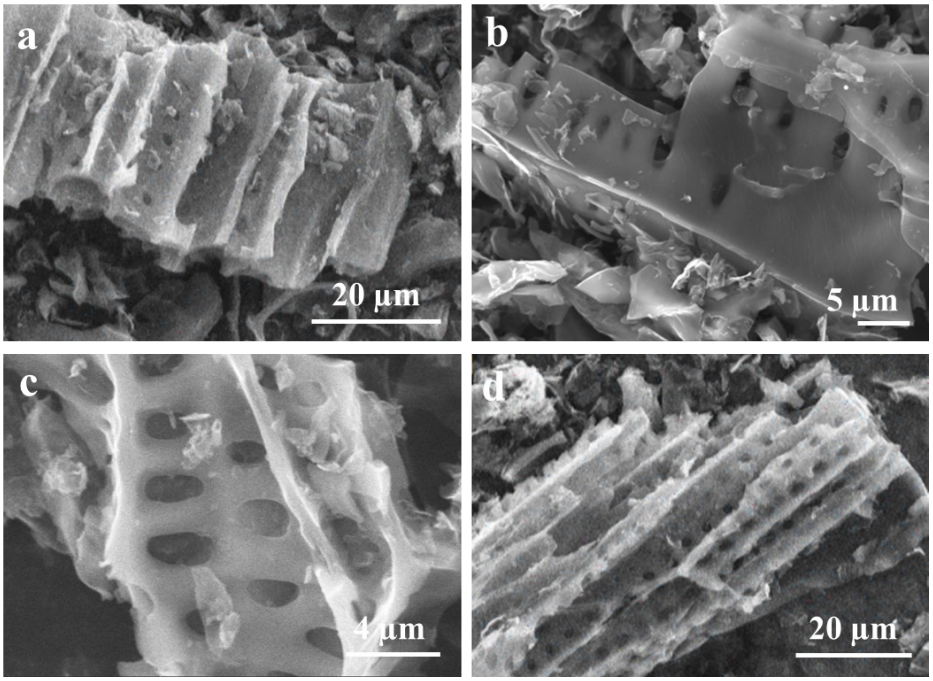

Figure S7 *SEM images of a) control, b)3DC-Au NPs, c) 3DC-Au NRs, and d) 3DC-Au NBPs, respectively.*

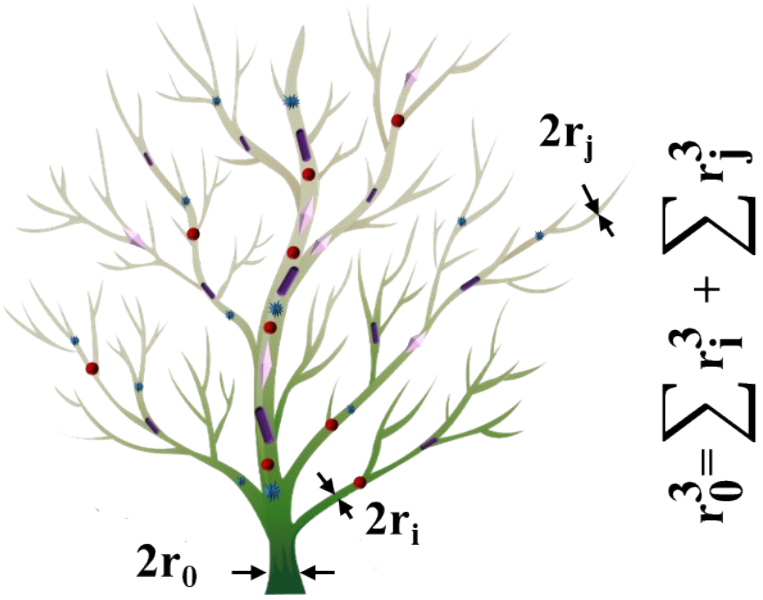

Figure S8 *Hierarchical models derived from Murray's plant systems.*

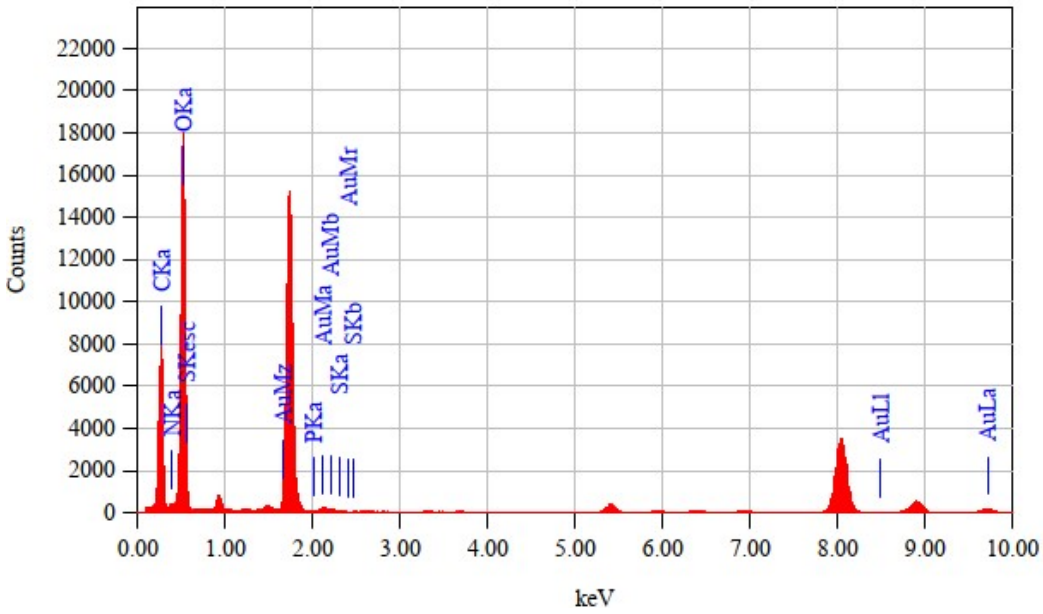

Figure S9 *EDS result of 3DC-Au NSs composite materials.*

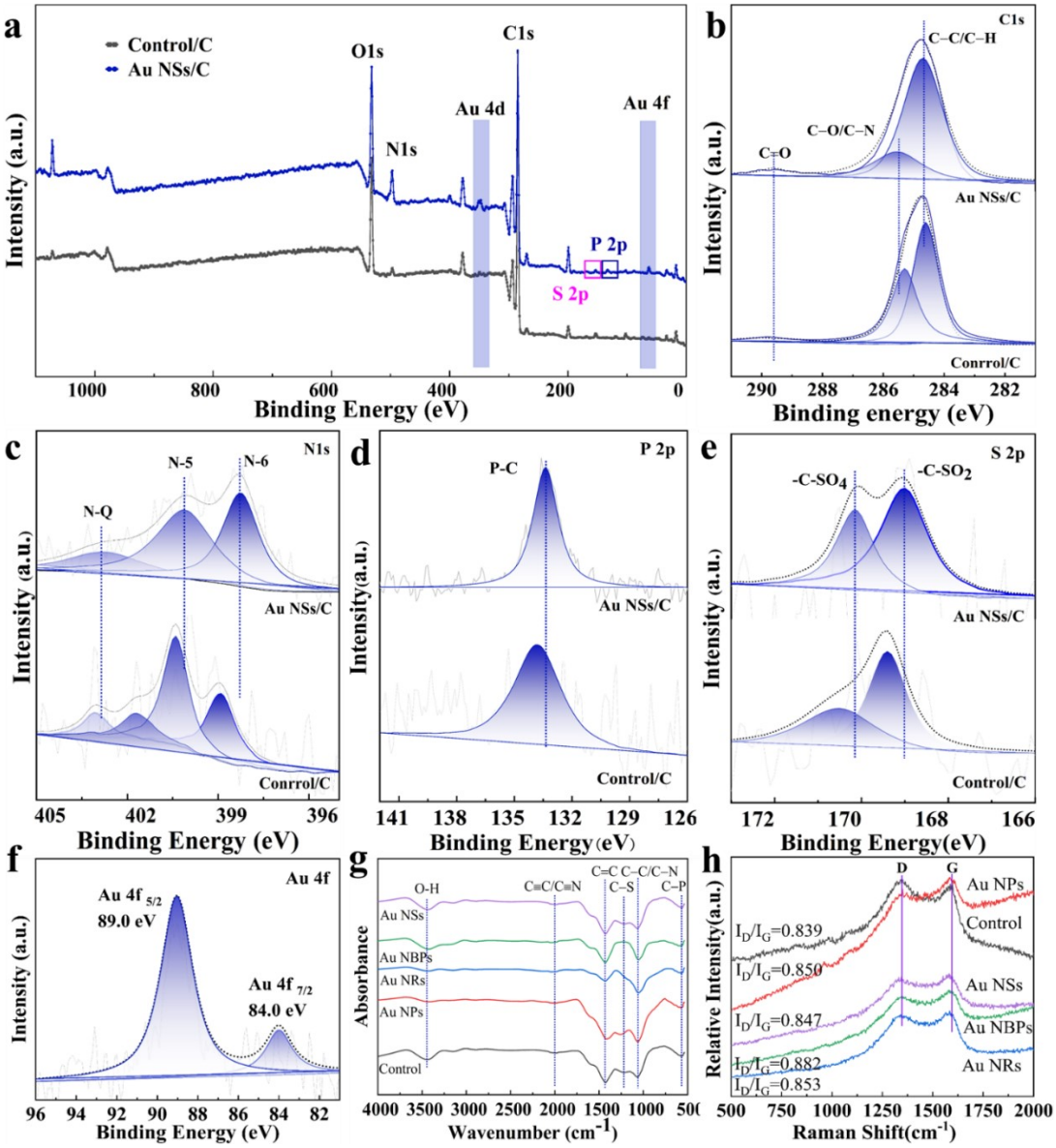

Figure S10 *a-f) XPS survey and high-resolution XPS spectra of C 1s, N 1s, P 2p, S 2p, and Au 4f of 3DC-Au NSs, respectively. g) Infrared spectrum and h) Raman spectrum.*

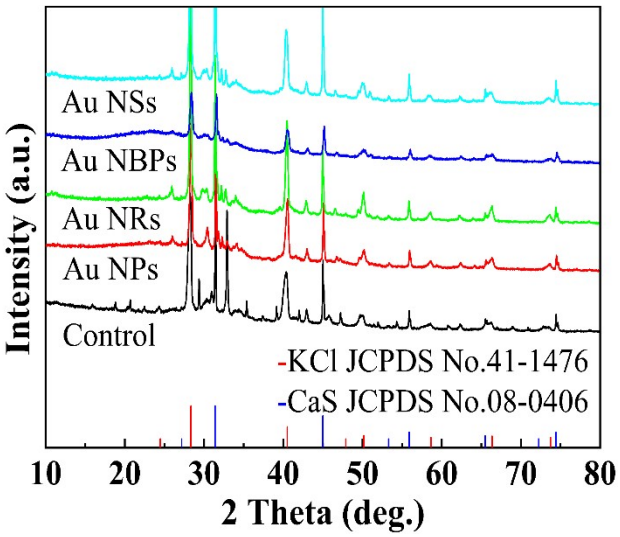

Figure S11 *XRD image of Control, 3DC-Au NPs, 3DC-Au NRs, 3DC-Au NBPs, and 3DC-Au NSs.*

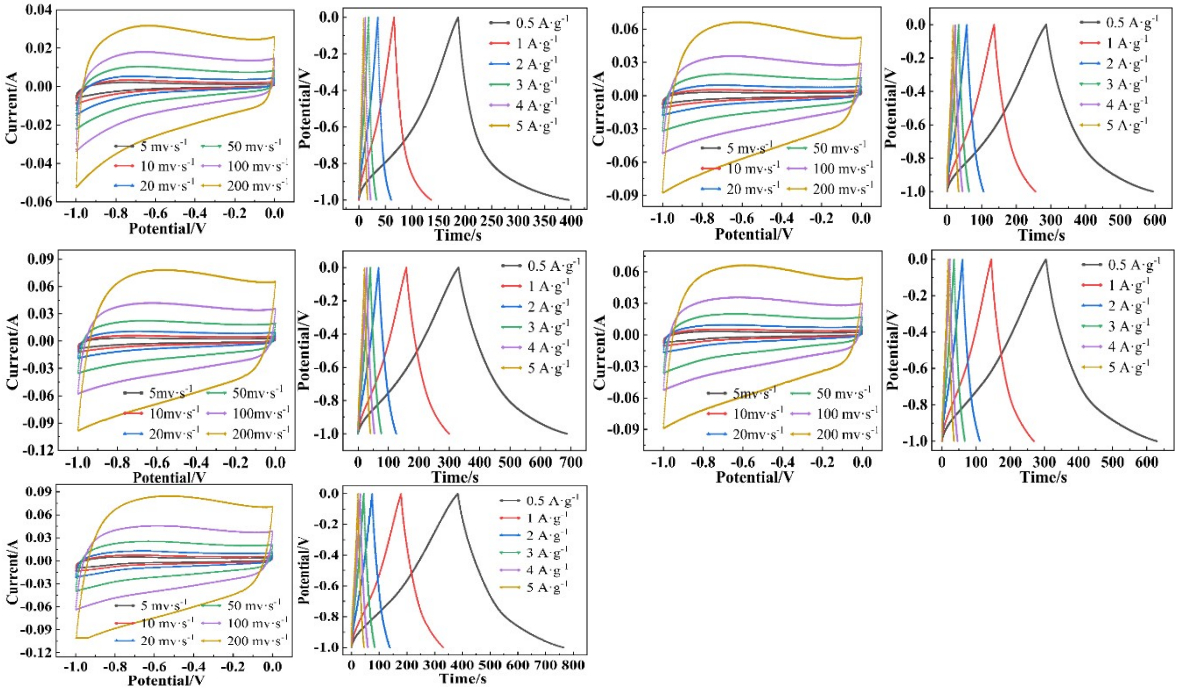

Figure S12 *Electrochemical performance of Control, 3DC-Au NPs, 3DC- Au NRs, and 3DC-Au NBPs, respectively. a, c, e, g) CV curves at different scan rate, b, d, f, h) GCD curves at different current density.*

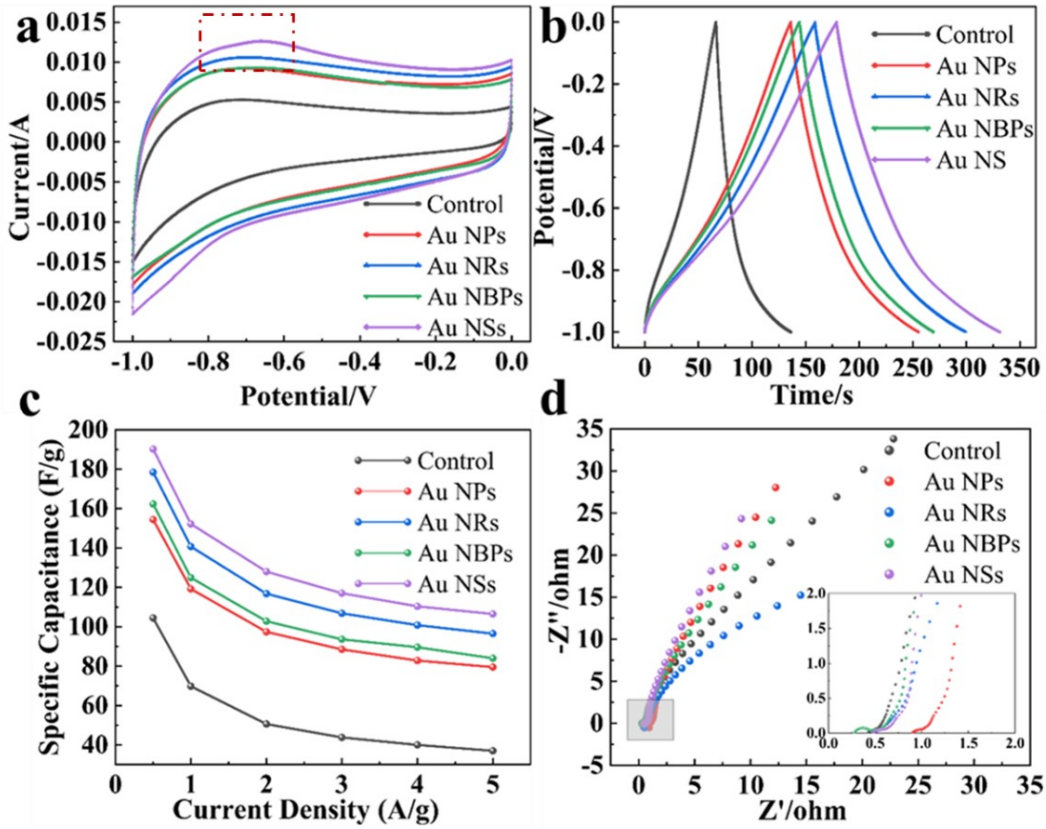

Figure S13 *Electrochemical performance of 3DC-control, 3DC-Au NPs, 3DC-Au NRs, 3DC-Au NBPs, and 3DC-Au NSs. a) CV curves at the scan rate of 50 mV·s^{-1}, b) GCD curves at the current density of 1* A·g^{-1}*, and c) comparisons of specific capacitances, and d) EIS spectra (inset: EIS spectra of the high-frequency region).*

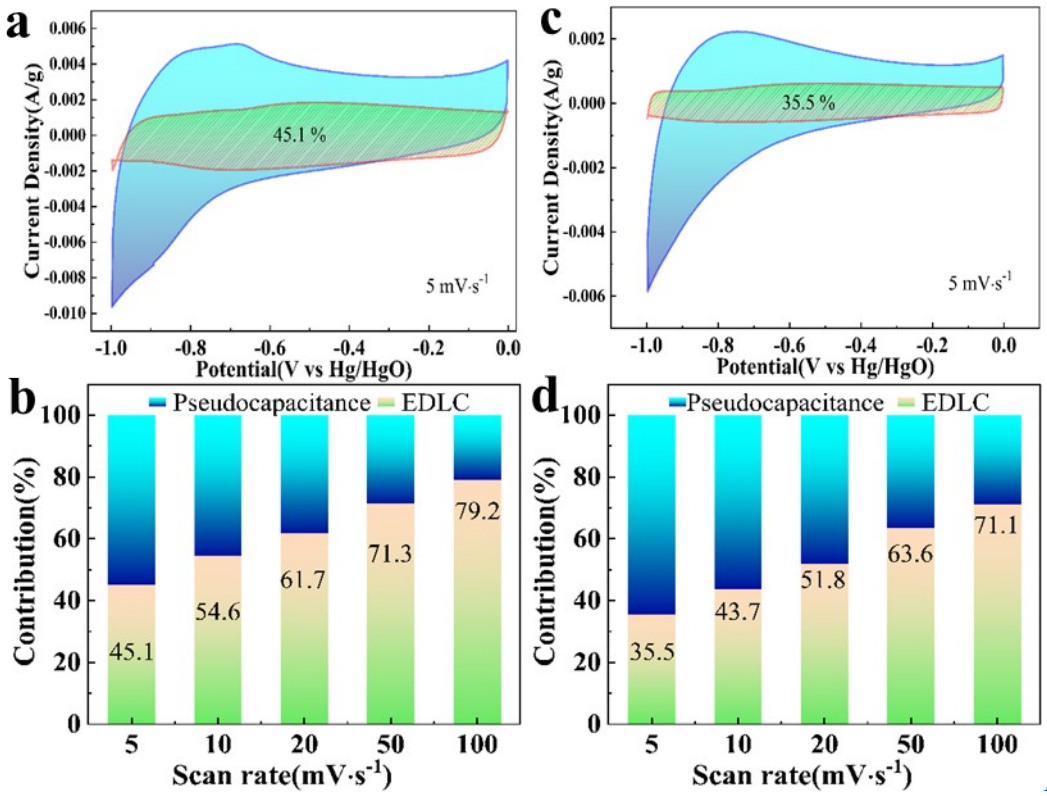

Figure S14 *Histogram shows the contribution of EDLC and pseudo capacitance for 3DC-Au NSs a-b) and control c-d) at various scan rates.*

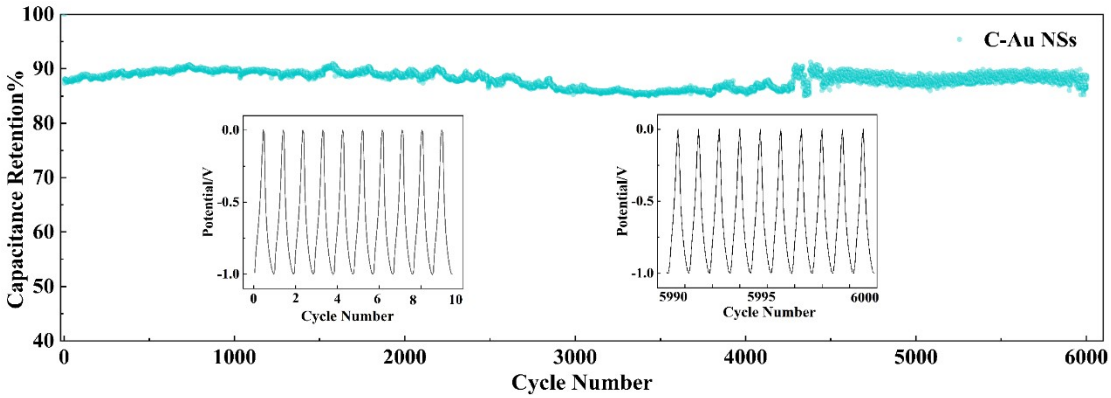

Figure S15 *Cycling stability of the C-Au NSs (0.5A/g). The inset shows the galvanostatic charge/discharge curves of the first and last 10 cycles.*

Table S1 *Pore structure parameters and specific surface area information of different samples.*

Samples	**Control**	**Au NPs**	**Au NRs**	**Au NBPs**	**Au NSs**
S_{BET} ($m^2 \cdot g^{-1}$)	212.18	288.29	254.47	223.05	199.75
Average pore size (nm)	3.432	3.626	2.485	5.059	2.610
V_p ($cm^3 \cdot g^{-1}$)	0.169	0.242	0.147	0.260	0.121
Median pore size of the microwell (nm)	0.9744	0.9519	0.636	0.8289	0.7022
V_{Mic} ($cm^3 \cdot g^{-1}$)	0.0798	0.1082	0.0891	0.0849	0.0705
V_{Mic}/V_p (%)	47.22	44.71	60.61	32.65	58.26

Table S2 The atomic compositions of different N, S, P species.

Relative	**N %**				**S %**		**P**
concentration	Pyridinic N-6	Pyrrolic N-5	Quaternary N-Q	Oxidized	−C− SO_2	−C− SO_4	P−C
Control	32.06	44.68	13.60	9.66	56.06	43.94	359.47
Au NSs	17.19	39.12	**43.68**	0	63.56	36.44	738.81

References

1 J. Turkevich, P. C. Stevenson, J. Hillier. A study of the nucleation-and-growt prgress in the synthsis of colloidal gold [J]. Discussions of the faraday society, 1951, 11: 55-75.

2 C. K. Tsung, X. S. Kou, Q. H. Shi, et al. Selective Shortening of Single-Crystalline Gold Nanorods by Mild Oxidation [J]. Journal of the American Chemical Society, 2006, 16(128): 5352-3.

3 Q. Li, X. L. Zhuo, S. Li, et al. Production of Monodisperse Gold Nanobipyramids with Number Percentages Approaching 100 % and Evaluation of Their Plasmonic Properties [J]. Advanced Optical Materials, 2015, 3(6): 801-12.

4 J. P. Xie, J. Y. Lee, D. I. C. Wang. Seedless, Surfactantless, High-Yield Synthesis of Branched Gold Nanocrystals in HEPES Buffer Solution [J]. Chemistry of Materials, 2007, 11(19): 2823-30.

5 Z. Jin, B. Wang, L. Ma, et al. Air pre-oxidation induced high yield N-doped porous biochar for improving toluene adsorption[J]. Chemical engineering journal, 2020, 385: 123843.

6 X. Yang, S. Zhao, Z. Zhang, et al. Pore structure regulation of hierarchical porous carbon derived from coal tar pitch via pre-oxidation strategy for high-performance supercapacitor[J]. Journal of Colloid and Interface Science, 2022, 614: 298-309.

7 G. G. Msemwa, M. G. Ibrahim, M. Fujii, et al. Phytomanagement of textile wastewater for dual biogas and biochar production: A techno-economic and sustainable approach[J]. Journal of Environmental Management, 2022, 322: 116097.